Preprint Title Multiple Fano resonances with flexible tunablity based on symmetry-breaking resonators

Authors Xiao b. Ren, Kun Ren, Ying Zhang, Cheng g. Ming and Qun Han

Article Type Full Research Paper

ORCID® iDs Kun Ren - https://orcid.org/0000-0003-4971-789X

Multiple Fano resonances with flexible tunablity based on symmetry-breaking resonators

Xiaobin Ren[1], Kun Ren[2,*], Ying Zhang[2], Chengguo Ming[1], Qun Han[2]

[1] College of Precision Instrument and Opto-electronics Engineering; Key Laboratory of Opto-electronics Information Technology, Ministry of Education, Tianjin 300072, China;
[2] School of Science, Tianjin University of Science and Technology, Tianjin 300222, China.
* Correspondence: renkun@tju.edu.cn.

Abstract: A symmetry-breaking nanostructure is proposed to achieve multiple Fano resonances. The nanostructure consists of an asymmetric ring resonator coupled to a plasmonic waveguide. The broken symmetry is introduced by deviating the centers of regular ring. New resonant modes those are not accessible to regular symmetric ring cavity are excited. Thus one asymmetric cavity can provide more than one resonant mode with the same mode order. As a result, the interval of Fano resonances is greatly reduced. By combining different rings with different asymmetric, multiple Fano resonances are generated. Those Fano resonances have different dependence on structural parameters due to their different physical origin. The resonance frequency and resonance peak number can be arbitrarily adjusted by changing the degree of asymmetry. This research may provide new opportunities to design on-chip optical devices with great tuning performance.

Keywords: Multiple Fano resonance, Tunable resonance, Symmetry-breaking, Off-centered ring resonators, Plasmonic waveguide, Surface plasmon polaritons

1. Introduction

Fano resonance originates from the interference of a discrete state and a continuum state [1,2]. Contrary to symmetric Lorentz lineshape, Fano profile is sharp and asymmetric. Due to its unique line shape and large induced field enhancements, Fano resonance has potential applications in sensor [3,4], demultiplexer [5], laser [6], filter [7], photoswitch [8], and so on.

Various structures have been designed to realize Fano resonance, including metallic nanoclusters [9,10], individual plasmonic dolmen nanocavity [11], ring/disk cavities [12,13], metamaterials and metasurfaces [14-16], and so on. In pariticular, as an important geometry, waveguide-cavity stucture are investigated at different platforms aiming for Fano resonance. For instance, Fano type transmission phenomenon is observed in photonic crystal (PhC) waveguide-cavity system [17,18]. The PhC waveguide is a line defect formed by removing a row of rods or air holes. The cavity is a point defect formed by reducing the radius of a single rod or removing an air hole. Fano profiles appear when partially reflecting elements are placed in PhC waveguide. The physical origin of Fano profile is the coupling of a discrete state (provided by cavity) to a continuum (provided by waveguide with partially reflectance).

In addtion to PhC waveguide, metal-dielectric-metal (MDM) waveguide has attracted intense research interests due to its ability of supporting surface plasmon polaritons (SPPs) and controlling light in deep subwavelength scale. MDM waveguide provides an effective approach to chip-scale photonic components [19-22]. Fano resonance has been acquired by MDM based waveguide-

cavity coupled systems [23,24]. In recent years, multiple Fano resonances have aroused interest [25-27]. Compared with single Fano resonance, multiple Fano resonances have more versatile and flexible applications, such as self-reference and multichannel sensing [25,26].

The generation of multi-Fano resonances is attributed to the existence of multiple discrete states. In most of published papers, high-order modes are excited in the same cavity [23,28]. Discrete states are provided by different modes from the same cavity, thus the resulting multiple Fano resonances belong to different orders of mode. As a result, the frequency interval of Fano resonance is usually very large, ranging about hundreds of nanometers. Recently, multiple Fano resonances are achieved with the aid of different cavities who provide several discrete states [26,29,30]. For instance, we have designed two U-shaped resonators for obtaining independent dual resonances [30].

In this paper, multiple Fano resonances are investigated and demonstrated in MDM waveguide-cavity coupled system. A symmetry-breaking ring cavity is proposed. Discrete states are obtained in the same cavity without exciting high-order cavity modes. Because of the same mode order, the interval of resonant frequency is reduced. The manipulation of Fano resonances are further discussed by adjusting the degree of asymmetry. More Fano peaks appear in the transmission spectrum by combining two symmetry-breaking cavities with different dimension.

2. Structure and Theory

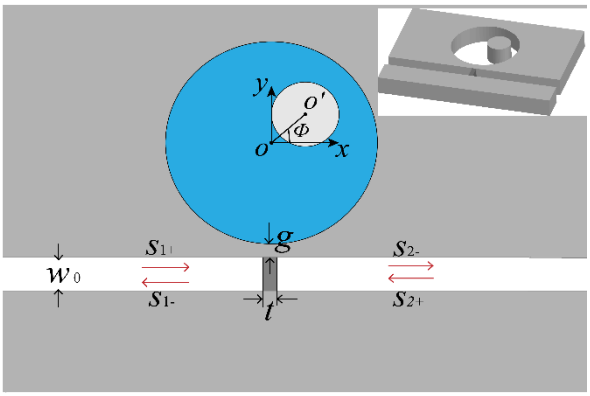

Figure 1 Schematic diagram of off-centered ring resonators (OCRR) side-coupled to MDM waveguide. The inset is the 3D view. The outer and inner radius of OCRR are *R* and *r*, respectively. The deviation of center points is denoted by *d*. The deviation angle is described by ϕ, which is the angle between the center connection and x-axis. The width of waveguide is W_0. The thickness of metal wall in waveguide is *t*. The coupling distance between disk resonator and upper stub is *g*.

Figure 1 shows the schematic diagram of MDM waveguide-cavity coupled system. The inset is the 3D view. The asymmetric cavity we designed is an off-centered ring resonator (OCRR). *O* and *O*' are the center of outer and inner circles, respectively. The distance between *O* and *O*' is denoted by *d*. When $d=0$, the cavity is a regular ring. When $d\neq0$, the regular ring becomes off-centered ring with the symmetry breaking. The deviation angle between the center connection and *x*-axis is described by ϕ. The deviation distance *d* and angle ϕ are parameters which are closely related to the degree of asymmetry. The radii of outer and inner ring cavity are *R* and *r*, respectively. OCRR is side-coupled to the waveguide with the gap *g*. The width of MDM waveguide is W_0. A metal wall with the thickness *t* is placed in MDM waveguide.

The grey parts in Fig. 1 stand for metal (ε_m). Both the metal wall and background metal are silver, whose complex relative permittivity is characterized by Drude model: $\varepsilon_m = \varepsilon_\infty - \omega_p^2/(\omega^2 + i\gamma\omega)$, where ω is the angular frequency of the incident light. The other parameters are ε_∞ = 3.7, bulk plasma frequency ω_p=1.38×10^{16} Hz, damping frequency γ=2.73×10^{13} Hz. The dielectrics in waveguide is air. The ring resonator is filled with dielectric (ε_d).

Temporal coupled mode theory (CMT) is used to analyze the transmission characteristics [30,31]. For the studied waveguide-resonator coupled system, the coupling coefficients between ring resonator and input (output) waveguide are denoted by κ_1 (κ_2). θ_1 and θ_2 are the phase shift of the coupling coefficient between ring resonator and input (output) waveguide. The decay rate due to the internal loss in the resonators is κ_i. The amplitudes of the incoming and outgoing waves in waveguide are denoted by S_{i+} and S_{i-} (i=1, 2).

The time evolution of normalized amplitude a of ring resonator can be expressed as:

$$\frac{da}{dt} = (j\omega_0 - \kappa_i - \kappa_1/2 - \kappa_2/2)a_1 + e^{-j\theta_1}\sqrt{\kappa_1}S_{1+} + e^{-j\theta_2}\sqrt{\kappa_2}S_{2+} \quad (1)$$

According to energy conservation, the amplitudes of the incoming and the outgoing waves in coupled waveguides satisfy the following relationships:

$$S_{2-} = t_{\mathrm{m}}S_{1+} - e^{-j\theta_2}\sqrt{\kappa_2}a \quad (2)$$

where t_{m} is the transmission coefficient for SPP passing through the waveguide with metal wall inside. It represents the direct coupling between input waveguide and output waveguide. If there is no metal wall in the waveguide, t_{m} is almost equal to 1. Eq. (2) can be rewritten as: $S_{2-} = S_{1+} - e^{-j\theta_2}\sqrt{\kappa_2}a$. If the transmission is completely forbidden due to metal wall, then t_{m}=0.

When an optical wave with frequency ω is launched only from the left port of the waveguide (S_{2+} = 0), the transmission of waveguide-resonator coupled system can be derived as:

$$T = \left|\frac{S_{2-}}{S_{1+}}\right|^2 = \left|t_{\mathrm{m}} - \frac{e^{j(\theta_1-\theta_2)}\sqrt{\kappa_1}\sqrt{\kappa_2}}{j(\omega-\omega_0)+\kappa_{\mathrm{i}}+(\kappa_1+\kappa_2)/2}\right|^2 \quad (3)$$

If the width of the input waveguide is the same as the width of the output waveguide, then $\theta_1 = \theta_2$ and $\kappa_1 = \kappa_2$.

In the case of no metal wall (corresponding to t_{m}=1), the transmission efficiency through the waveguide-resonator system is described by:

$$T = \left|1 - \frac{\kappa}{j(\omega-\omega_0)+\kappa_{\mathrm{i}}+\kappa}\right|^2 = \left|\frac{j(\omega-\omega_0)+\kappa_{\mathrm{i}}}{j(\omega-\omega_0)+\kappa_{\mathrm{i}}+\kappa}\right|^2 \quad (4)$$

The above expression agrees with Eq. (3) in Ref. [32] which deals with a waveguide with a side-coupled nanocavity. Eq. (4) shows at the resonance frequency ω_0, the transmission reaches minimum: $T_{\mathrm{min}} = |\kappa_{\mathrm{i}}/(\kappa_{\mathrm{i}}+\kappa)|^2$. This means there would be a narrow transmission dip. If there is no internal loss κ_{i}, we have $T_{\mathrm{min}} = 0$.

When the transmission coefficient t_{m} is relatively low and closes to zero, Eq. (3) can be expressed as:

$$T = \left|-\frac{\kappa}{j(\omega-\omega_0)+\kappa_{\mathrm{i}}+\kappa}\right|^2 \quad (5)$$

Eq. (5) shows that the maximum transmission T_{max} happens when $\omega=\omega_0$: $T_{\mathrm{max}} = |\kappa/(\kappa_{\mathrm{i}}+\kappa)|^2$. The transmission spectrum has a peak around the resonance frequency ω_0. If there is no internal loss

κ_i, we have $T_{max} = 1$.

3 Results and Discussion

Numerical simulation are performed by COMSOL Multiphysics. The width of waveguide is W_0=50 nm, the gap between waveguide and resonator is g=10 nm. The outer and inner radius of ring are R=155 nm and r= 55 nm, respectively. The deviation angle ϕ=0^0 and deviation distance d=0.

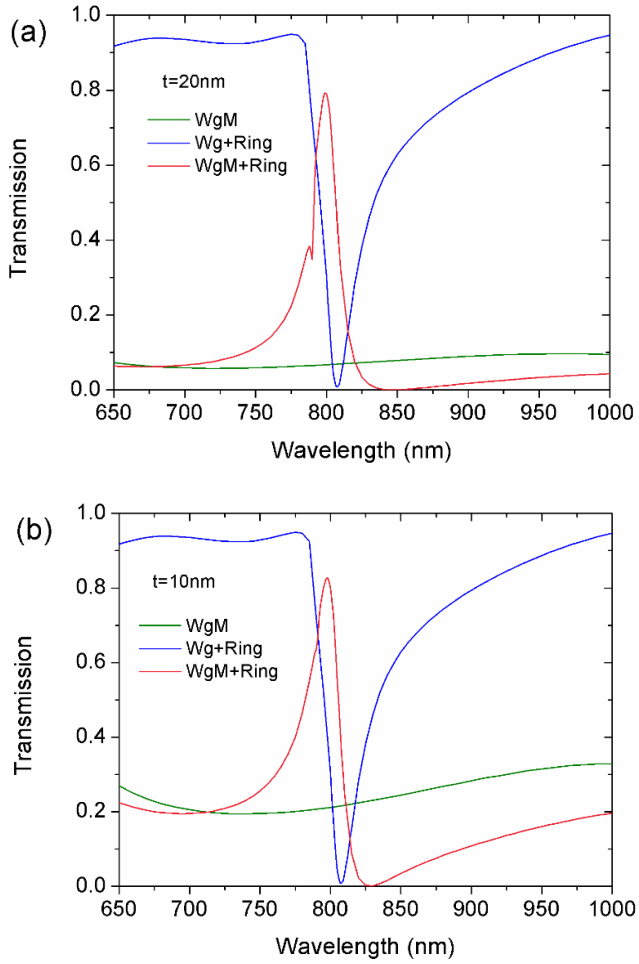

Figure 2 Transmission spectra for different structures. (a) t=10nm, and (b) t=20nm. The other parameters are R=155 nm, r= 55 nm and ϕ=0^0.

Figure 2 shows the transmission spectra for designed waveguide-resonator coupled system. Different thickness of metal wall t is studied. When a metal wall is placed in a MDM waveguide, the transmittance is low within a wide spectrum range, as shown by green curve. The continuum state is provided by the waveguide with a metal wall inside (WgM). When a ring side-coupled to an ordinary waveguide (Wg+Ring), a narrow dip at 807 nm appears in the transmission spectrum, as shown by blue curve. This dip means that the discrete state can be provided by the side-coupled ring cavity. For the system consisting of a ring and a waveguide with inserted metal wall (WgM+Ring), a transmission peak appears around 800 nm, shown by red curve. The transmission profile looks asymmetric. In particular, when metal thickness t=10 nm, the asymmetric lineshape is more obvious, as shown in Fig. 2(b). We regard this resonance as Fano resonance, which arises from the interference of ring resonant mode and waveguide mode. From Fig.2, we infer that the position of Fano peak is more determined by the ring cavity.

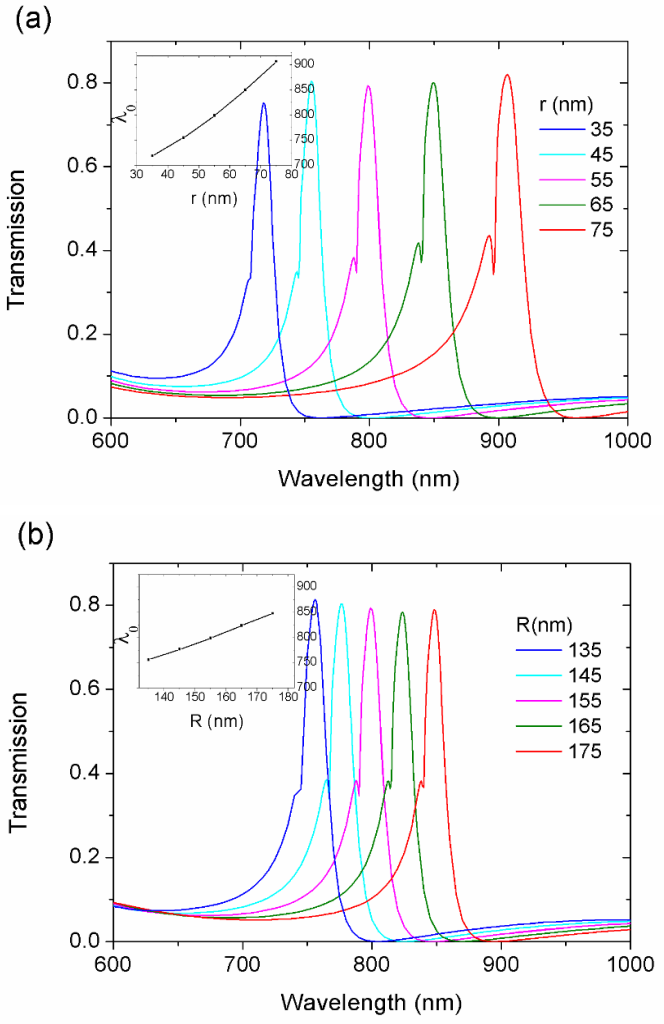

Figure 3 Transmission spectra at different structural parameters: (a) inner radius *r*, (b) outer radius *R*.

In the following, the influence of ring cavity on Fano resonance is investigated. The evolution of transmission spectra with the inner radius is given in Fig. 3(a). It is seen that transmission peaks move to long wavelength side with the increase of inner radius *r*. The inset shows the resonance wavelength λ_0 as a function of radius *r*. It is obvious that the resonance wavelength is proportional to inner radius *r*. This can be explained by the resonance function. The resonance wavelengths are determined by:

$$\lambda_{0,m} = \mathrm{Re}(n_{eff})L_{eff}/m \tag{1a}$$

$$L_{eff} = 2\pi R_{eff} = \pi(R+r) \tag{2b}$$

where L_{eff} is the effective length of ring resonator. *m* is an integer corresponding to the mode order. n_{eff} means effective index, which can be obtained from dispersion equation [33].

Fig. 4 presents the effective index n_{eff} as a function of wavelength at different ring width *W*. It is observed that the larger the width *W*, the lower the effective index n_{eff}. Combining Eq. (1) and Fig.4, we conclude that the resonance frequency of ring depends on the radii and the width of the ring.

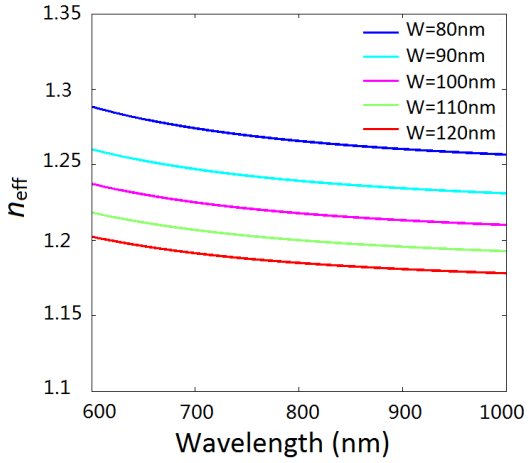

Figure 4 Effective refraction index n_{eff} Verus wavelength at different ring width *W*.

When the inner radius *r* increases from 35 nm to 75 nm, the effective length L_{eff} becomes larger, and meanwhile, the ring width decreases from 120 nm to 80 nm, which leads to bigger index n_{eff}. As a result, both L_{eff} and n_{eff} increase with the increase of radius *r*. According to Eq. (1), the corresponding resonance wavelength will become longer. The simulation shows the Fano peak has a redshift, which is consistent with the analysis.

Fig. 3(b) shows the evolution of transmission with the outer radius *R*. The inset shows the resonance wavelength λ_0 as a function of *R*. It is clear that with the increase of outer radius *R*, transmission peak moves to long wavelength, too. Note that the redshift in Fig. 3(b) is smaller compared with that in Fig. 3(a). We attribute this phenomenon to different impact of L_{eff} and n_{eff} on transmission. When outer radius *R* increases from 135 nm to 175 nm, ring width *W* increases from 80 nm to 120 nm. Because n_{eff} is inversely proportional to width *W*, bigger *W* will result in smaller n_{eff}. On the contrary, the effective length L_{eff} increase with *R*. The blueshift of resonance wavelength caused by decreased n_{eff} will partially offset the redshift of resonance wavelength caused by increased L_{eff}. This is the reason why the shift of resonance peak in Fig. 3(b) is less than that in Fig. 3(a).

We have demonstrated that the ring is the key component for controlling the resonant frequency. In the following, we break the symmetry of ring resonator and investigate the impact of symmetry-breaking on Fano resonance. The symmetry-breaking is introduced by deviating center points *O* and *O*'. When deviation distance *d* is greater than 0, a regular ring becomes off-centered ring. Fig. 5(a) displays the transmission spectra at *d*=80 nm with varying angle ϕ. When rotating ϕ counterclockwise, new transmission peak 2 appears on the left side of initial peak 1. With the increase of ϕ, the amplitude of peak 2 gradually increases while the amplitude of peak 1 gradually decreases. When ϕ reaches to 90^0, resonance 1 is totally suppressed and only resonance 2 exists. When rotating ϕ clockwise from 0^0 to -90^0, similar phenomenon is observed, as shown in Fig. 5(c). New resonance peak 2 appears and gradually increase its amplitude. Meanwhile, peak1 is gradually suppressed. We note that the linewidth of peak 2 in Fig. 5(a) and Fig. 5(b) differ. The electric field distributions for peak 1 and 2 at ϕ= 45^0 and -45^0 are shown in Fig. 5(b) and Fig. 5(d), respectively. It is observed that peak 1 and peak 2 belong to the first mode order but their field patterns have different symmetry. It is the symmetry-breaking of the ring that leads to the change in the field distribution. The redistribution of field intensity would affect the coupling strength

between ring resonator and waveguide. As a result, the linewidth of resonance peaks differ.

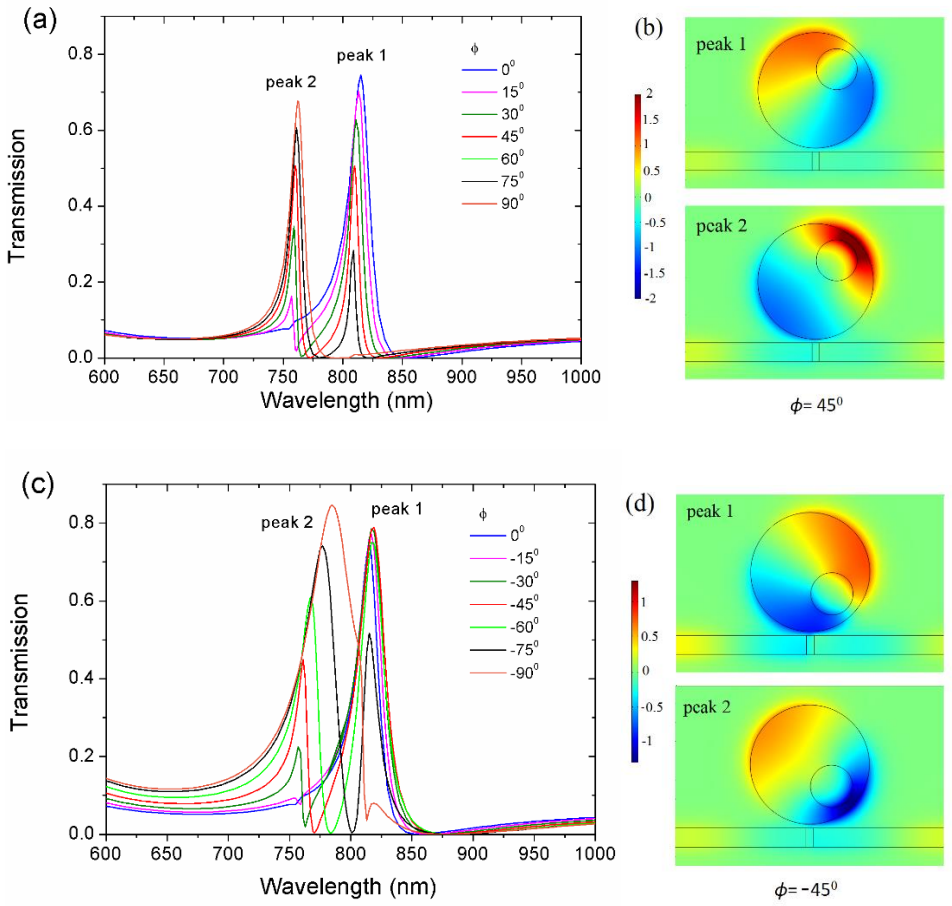

Figure 5 The evolution of transmission spectra with angle ϕ varying (a) from 0^0 to 90^0, (b) from 0^0 to -90^0. The electric field distribution for peak I and II at (b) $\phi = 45^0$ (810nm and 760nm), and (d) $\phi = -45^0$ (819nm and 761nm). The other parameters are R=155 nm, r= 55 nm, and the deviation distance d=80 nm.

Figure 6 shows the evolution of transmission spectra at different deviation distance d. For clarity, only there angles ϕ are plotted. New resonance peak 2 can be observed when d equals 40 nm and 80 nm. Comparing Fig. 6(a) with Fig. 6(b), we find that as d increases, resonance 1 has a redshift while resonance 2 has a blueshift. The opposite shift leads to increased wavelength interval between two peaks at larger d. The reason is attributed to greater asymmetry caused by larger deviation distance d.

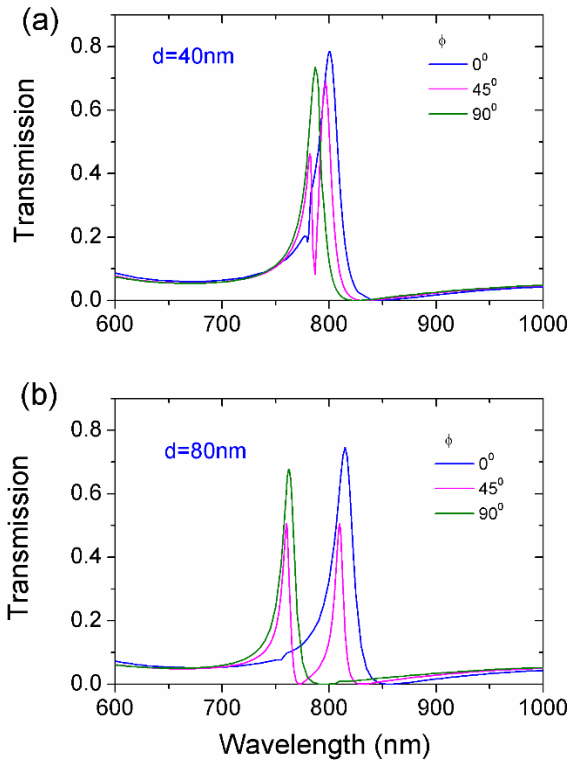

Figure 6 The evolution of transmission spectra with angle ϕ. The deviation distance is (a) d=40 nm, (b) d=80 nm. The other parameters are R=155 nm, r= 55 nm.

We have demonstrated by Fig.5 and Fig.6 that the dual resonances can be obtained by breaking the symmetry of ring resonator. And the resonance frequency and number of peak can be tailored through altering the degree of asymmetry, i.e. the deviation distance d and deviation angle ϕ. Now another ring is placed at the other side of the waveguide with the gap distance g=10nm. The outer and inner radius of the second ring are R_2=155 nm and r_2=75 nm, respectively. The deviation angle ϕ_2=-45^0 and deviation distance d_2=55nm. Fig.7 shows the transmission spectra when the deviation angle ϕ of the first ring changes. Different deviation distances d are considered. Two new peaks located at 880nm and 925nm are observed in addition to the original resonance peaks around 800nm. For clarity, we refer new emergent resonance peaks as band II and original resonance peaks as band I. In the presence of two resonators, the resonances of band I in Fig.7 show the same characteristic as the resonances in Fig.6. At ϕ=0^0 and ϕ=90^0, only one peak is excited. At ϕ=45^0 both peak 1 and peak 2 are excited. Furthermore, the larger d, the more distinct wavelength interval between peak 1 and 2 is. However, the resonances of band II keep unchanged as ϕ varies. This different behavior demonstrate that band I origins from the coupling of 1st ring and waveguide. Therefore band I depends on parameters of 1st ring and is immune to 2nd ring.

The impact of deviation angle ϕ_2 of 2nd ring on transmission is also investigated. The transmission spectra with varied ϕ_2 at different deviation distance d_2 are plotted in Fig.8. Similar phenomenon is observed. One or two resonances of band II appear as deviation angle ϕ_2 changes. Furthermore, the wavelength interval between resonance peak 3 and 4 get larger with increased d. However, the resonances of band I are independent of ϕ_2. This behavior indicates that the resonances of band II originate from the coupling of 2nd ring and waveguide.

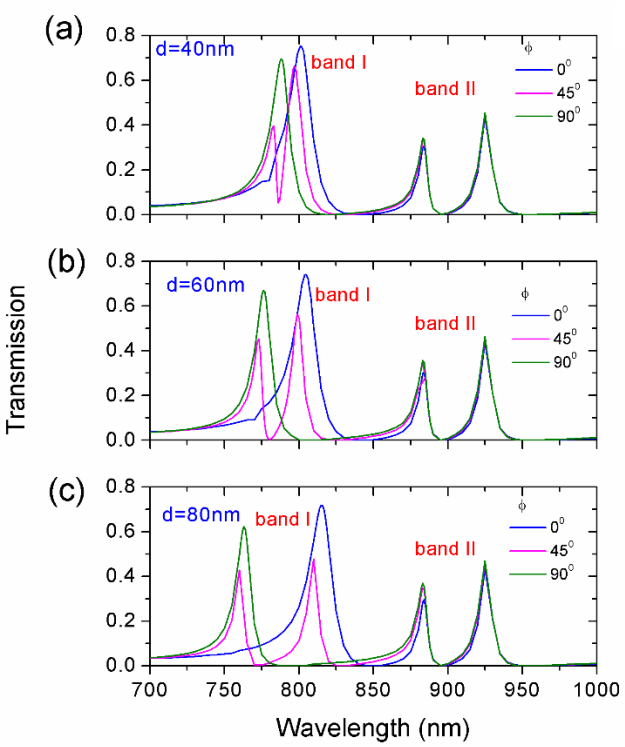

Figure 7 The evolution of transmission spectra with deviation angle ϕ of initial ring. The deviation distances is (a) d=40 nm, (b) d=60 nm, (c) d=80 nm. The other parameters of initial ring are R=155 nm, r= 55 nm. The deviation angle ϕ=45^0 and deviation distance d=80nm. The parameters for 2nd ring are R_2=155 nm, r_2= 75 nm, d_2=55nm, ϕ_2=-45^0.

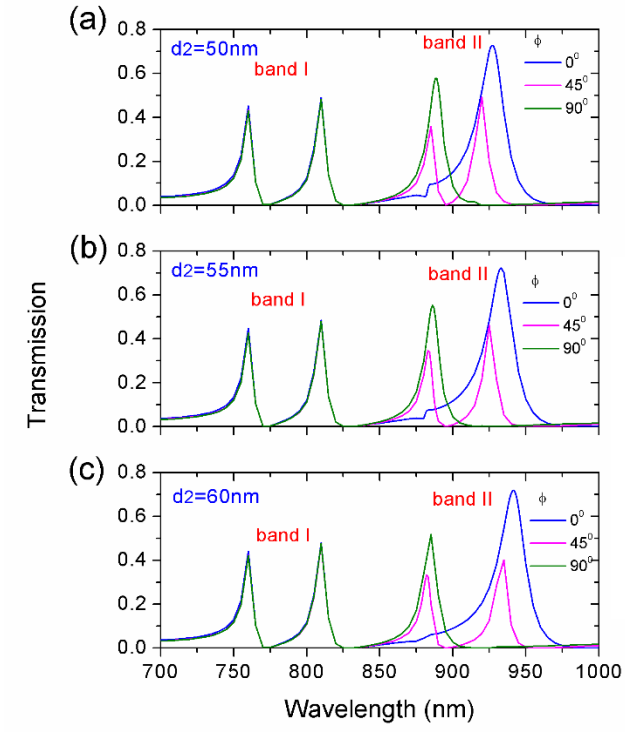

Figure 8 The evolution of transmission spectra with deviation angle ϕ_2 of 2nd ring. The deviation distance d_2 is (a) d_2 =50 nm, (b) d_2 =55 nm, (c) d_2 =60 nm. The other parameters of 2nd ring are R_2=155 nm, r_2= 75 nm. The parameters for initial ring are R=155 nm, r= 55 nm, d=80nm, ϕ=45^0.

From Fig.7 and Fig.8, we know that the resonances of band I is determined by the 1st ring and the resonances of band I depend on the 2nd ring. This different dependence provides good opportunity to separately tune multiple Fano resonances. Fig. 9 shows the transmission spectra with different parameters of two ring resonators. The numbers in each subfigure stand for the value of (d, ϕ) and (d_2, ϕ_2). The outer and inner radii are constant. R=155 nm, r=55 nm, R_2=155 nm and r_2=75 nm. It is seen that dual, triple and even quadruple Fano type transmission are obtained by separately adjusting the deviation distance and deviation angle of each off-centered ring. In particular, there are triple peaks in Fig. 9(b)-(e) but their resonant frequencies and frequency interval are not the same. This shows that multiple resonances can be arbitrarily tailored by changing the degree of asymmetry.

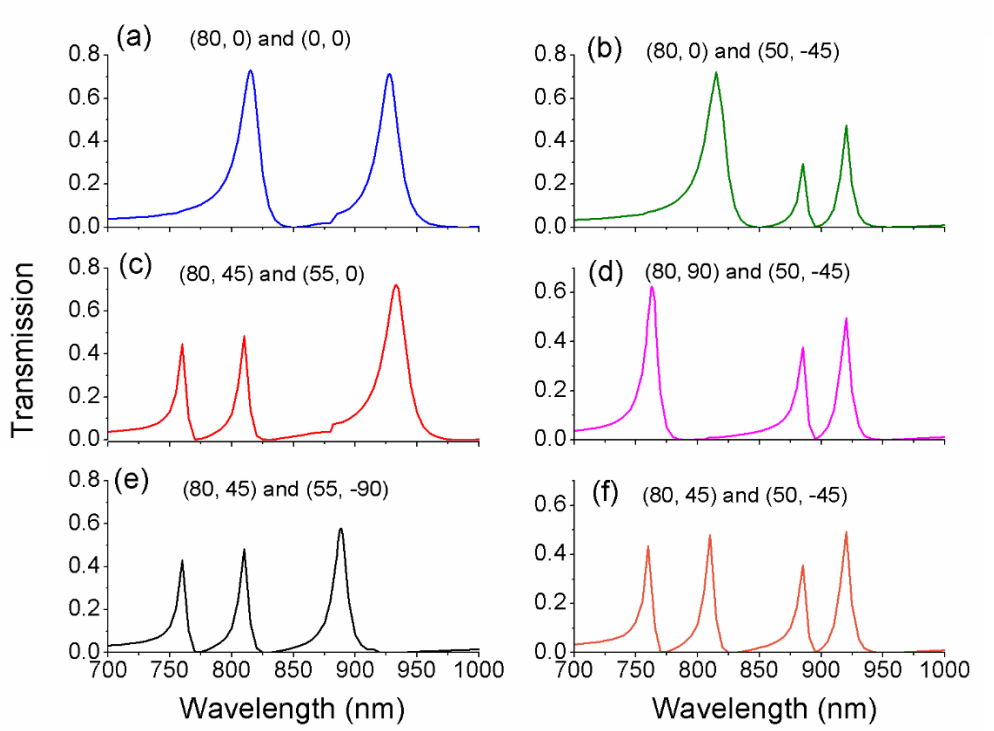

Figure 9 The evolution of transmission spectra with different parameters (d, ϕ) and (d_2, ϕ_2) of two off-centered rings.

We have demonstrated that the radius of ring is a key factor for Fano resonance in Fig.2 and Fig.3. The impact of radius on multiple Fano resonances in the presence of two rings is further investigated. Fig. 10 shows the evolution of transmission spectra with different inner radii r and r_2. Fano resonant peaks have a redshift with the increase of inner radius. Nevertheless, band I is most affected by r, and band II is most affected by r_2. Multiple resonances can be independently tuned by changing the inner radius. Therefore one can regulate the frequency interval of resonance between band 1 and band II. Likewise, we find that the outer radius has an effect on the resonant frequency. In Fig.9 and Fig.10, we demonstrate that Fano resonance can be flexibly controlled by the structural parameters (R, r, d, ϕ) and (R_2, r_2, d_2, ϕ_2). These results are great benefit to tunable integrated photonic devices.

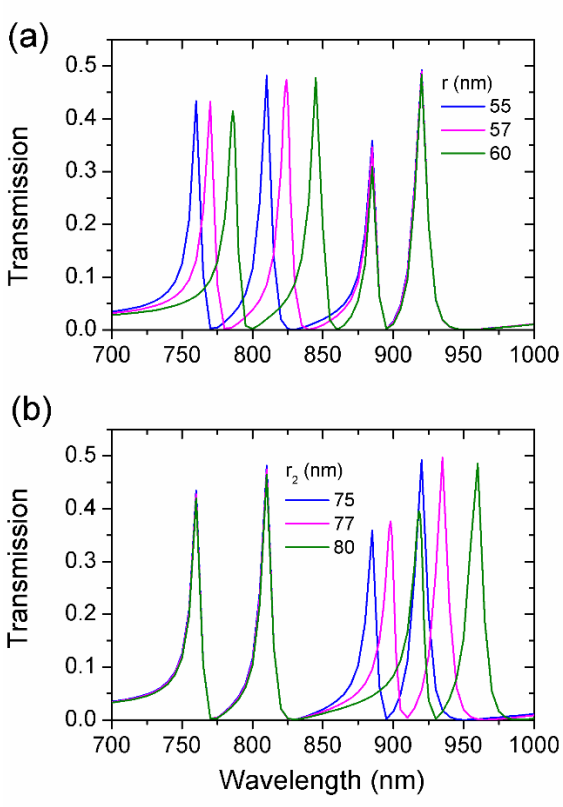

Figure 10 The evolution of transmission spectra with different radius (a) r at r_2= 75 nm, (b) r_2 at r= 55 nm. The fixed parameters for initial ring are R=155 nm, d=80nm, ϕ=45^0. The fixed parameters of 2nd ring are R_2=155 nm, d_2 =50 nm, ϕ_2=-45^0.

4. Conclusion

We have demonstrated multiple Fano resonances in off-centered ring resonators-waveguide system. By breaking the symmetry of ring resonator, new resonant modes those are not achieved by regular concentric ring resonators are excited. Degrees of asymmetry are adjusted by changing the deviation distance and deviation angle of asymmetric ring resonator. Dual, triple and even quadruple Fano type transmission are arbitrarily tailored. The frequency interval of multiple Fano resonances can be tuned. The results may provide good guidance for designing flexibly tunable integrated photonic devices.

Acknowledgements: This work was supported by the National Natural Science Foundation of China (11104200) and Natural Science Foundation of Tianjin (18JCYBJC17000)。

Conflicts of Interest: The authors declare no conflict of interest.

References

1. U. Fano, “Effects of configuration interaction on intensities and phase shifts,” Phys. Rev. **124**(6), 1866–1878 (1961).
2. Luk'yanchuk, B.; Zheludev, N. I.; Maier, S. A.; Halas, N. J.; Nordlander, P.; Giessen, H.; Chong, C. T. *Nature Materials* **2010,** *9* (9), 707-715.

3. Huang, C. Y.; Chang, H. C. *Ieee Photonics Journal* **2019,** *11* (1).
4. Wu, C.; Khanikaev, A. B.; Adato, R.; Arju, N.; Yanik, A. A.; Altug, H.; Shvets, G. Fano-resonant asymmetric metamaterials for ultrasensitive spectroscopy and identification of molecular monolayers. Nat. Mater. 2011, 11, 69–75.
5. Chen, J. J.; Li, Z.; Li, J.; Gong, Q. H. *Optics Express* **2011,** *19* (10), 9976-9985.
6. Wang, L.; Qu, J.; Song, J.; Xian, J. *Plasmonics* **2017,** *12* (4), 1145-1151.
7. Zhao, W. Y.; Leng, X. D.; Jiang, Y. Y. *Optics Express* **2015,** *23* (5), 6858-6866.
8. Manjappa, M.; Srivastava, Y. K.; Cong, L. Q.; Al-Naib, I.; Singh, R. *Advanced Materials* **2017,** *29* (3).
9. Lassiter, J. B.; Sobhani, H.; Fan, J. A.; Kundu, J.; Capasso, F.; Nordlander, P.; Halas, N. J. *Nano Letters* **2010,** *10* (8), 3184-3189.
10. Truong Khang, N.; Truong Duy, L.; Phuc Toan, D.; Le, K. Q. *Journal of the Optical Society of America B-Optical Physics* **2017,** *34* (3), 668-672.
11. Verellen, N.; Sonnefraud, Y.; Sobhani, H.; Hao, F.; Moshchalkov, V. V.; Van Dorpe, P.; Nordlander, P.; Maier, S. A. *Nano Letters* **2009,** *9* (4), 1663-1667.
12. Hao, F.; Sonnefraud, Y.; Van Dorpe, P.; Maier, S. A.; Halas, N. J.; Nordlander, P. *Nano Letters* **2008,** *8* (11), 3983-3988.
13. Cetin, A. E.; Altug, H. *Acs Nano* **2012,** *6* (11), 9989-9995.
14. Huang, W. X.; Guo, J. J.; Wang, M. S.; Zhao, G. R. *Physics Letters A* **2017,** *381* (10), 909-912.
15. Campione, S.; Liu, S.; Basilio, L. I.; Warne, L. K.; Langston, W. L.; Luk, T. S.; Wendt, J. R.; Reno, J. L.; Keeler, G. A.; Brener, I.; Sinclair, M. B. *Acs Photonics* **2016,** *3* (12), 2362-2367.
16. Muhammad, N.; Ouyang, Z. B.; Liu, Q.; Tang, X. P.; Deng, Z. L.; Khan, A. D. *Journal of Materials Science* **2019,** *54* (8), 6301-6309.
17. Fan, S. H. *Applied Physics Letters* **2002,** *80* (6), 908-910.
18. Zhao, Y.; Qian, C.; Qiu, K.; Tang, J.; Sun, Y.; Jin, K.; Xu, X. *Scientific Reports* **2016,** *6*.
19. Abdulnabi, S. H.; Abbas, M. N. *Journal of Nanophotonics* **2019,** *13* (1).
20. Lu, H.; Yue, Z. Q.; Zhao, J. L. *Optics Communications* **2018,** *414*, 16-21.
21. Dong, L. R.; Xu, X. M.; Li, C. J.; Guo, Y.; Sun, K. H.; Ding, Y. P. *Optics Communications* **2018,** *410*, 751-755.
22. Yang, J. H.; Song, X. K.; Yang, S.; Cui, L. N.; Yu, L. *Journal of Physics D-Applied Physics* **2017,** *50* (32).
23. Ren, X. B.; Ren, K.; Cai, Y. X. *Applied Optics* **2017,** *56* (31), H1-H9.
24. Tang, Y.; Zhang, Z. D.; Wang, R. B.; Hai, Z. Y.; Xue, C. Y.; Zhang, W. D.; Yan, S. B. *Sensors* **2017,** *17* (4).
25. Ren, X. B.; Ren, K.; Ming, C. G. *Sensors* **2018,** *18* (5).
26. Guo, Z. C.; Wen, K. H.; Hu, Q. Y.; Lai, W. H.; Lin, J. Y.; Fang, Y. H. *Sensors* **2018,** *18* (5).
27. Chen, Z.; Li, H. J.; He, Z. H.; Xu, H.; Zheng, M. F.; Zhao, M. Z. *Applied Physics Express* **2017,** *10* (9).
28. Li, C.; Li, S. L.; Wang, Y. L.; Jiao, R. Z.; Wang, L. L.; Yu, L. *Ieee Photonics Journal* **2017,** *9* (6).
29. Shi, X. L.; Ma, L. J.; Zhang, Z. D.; Tang, Y.; Zhang, Y. J.; Han, J. Q.; Sun, Y. Q. *Optics Communications* **2018,** *427*, 326-330.
30. Ren, K.; Ren, X. B.; He, Y. M.; Han, Q. *Beilstein Journal of Nanotechnology* **2019,** *10*, 247-255.
31. Deng, Y.; Cao, G. T.; Wu, Y. W.; Zhou, X. Q.; Liao, W. H. *Plasmonics* **2015,** *10* (6), 1537-1543.
32. Lu, H.; Liu, X. M.; Gong, Y. K.; Wang, L. R.; Mao, D. *Optics Communications* **2011,** *284* (10-11), 2613-2616.
33. Dionne, J. A.; Sweatlock, L. A.; Atwater, H. A.; Polman, A. *Physical Review B* **2006,** *73* (3).